43rd AIAA/ASME/SAE/ASEE Joint Propulsion Conference & Exhibit
8 - 11 July 2007, Cincinnati, OH

AIAA 2007-5635

Representation of Chemical Kinetics by Artificial Neural Networks for Large Eddy Simulations

Baris A. Sen* and Suresh Menon†

School of Aerospace Engineering, Georgia Institute of Technology,
Atlanta, GA, 30332-0150, USA

This paper discusses an approach to incorporate Artificial Neural Network (ANN) based kinetics modeling into Large-Eddy Simulation (LES) of reactive flows. The emphasis has been spent for replacing stiff ordinary differential equation (ODE) solvers with ANN for chemical kinetics calculations. A back-propagation type of an ANN code has been developed and its performance has been tested in laminar and turbulent methane/air and syngas/air premixed combustion processes. The ANN is trained using an independent premixed flame calculation and then used as is in the LES. Results indicate that the accuracy of ANN predictions for turbulent flow computations highly depend on the initial training data-set. If well trained, ANN can succesfully predict the chemical state-space using less memory than a conventional look-up table approach and in a computationally efficient manner than the stiff ODE solvers.

I. Introduction

Accurate prediction of the scalar and the vectoral fields inside the combustion chamber of a gas turbine engine is a challenging task and requires the solution of a three dimensional, highly unsteady, turbulent reactive flow problem. Direct Numerical Simulation (DNS) of the high Reynolds number flows is not affordable yet, since the grid resolution dictated by the solution methodology far more exceeds the current computer capabilities.[1] Therefore, there is a need for simulation models that would decrease the computational cost without significant reduction in accuracy.

In the realm of reactive flow computations, great effort has been spent to capture the time dependent processes by LES computations. In order to capture the changes in the species composition state-space due to the chemical reactions a stiff non-linear ODE system must be solved. The size of the equation system is determined by the number of species simulated. Thus, for a detailed reaction mechanism, the chemical kinetics calculations are very time consuming and their application to the engineering problems may be restricted similar to DNS due to the need for computational resources. Relatively smaller chemical kinetics mechanisms obtained by using partial equilibrium and/or steady state assumptions are more widely used than the more detailed mechanisms. However, the reduction process from the detailed to the reduced mechanisms have to be handled carefully in order to yield a match between the range of applicability of the assumptions and the operating conditions of the problem.[2]

Remedies for speeding-up chemical kinetics calculations exist in the literature, such as Intrinsic Low-Dimensional Manifolds (ILDM)[2] and In-Situ Adaptive Tabulation (ISAT) methodologies.[3] ILDM requires generation of a multi dimensional look-up table prior to starting the flow computations. The number of resolved states by ILDM should be sufficient enough to include all the possible states that may occur during the simulation. Since this information is not known *apriori*, huge tables can be generated, which would require large memory for table storage.[4] ISAT, on the other hand, is no different than direct integration of the chemical equation system in the early stages of the simulation, since the look-up table is generated as simulation proceeds.

*Graduate Research Assistant, AIAA Student Member.
†Professor, AIAA Associate Fellow.

Another solution is ANN[5] methodology, which is a relatively new technique in the area of chemical kinetics and its aplicability has not been tested fully yet for turbulent reactive flow applications. ANN is widely used for function approximation, classification, time series prediction, filtering, data association and optimization,[6] and is a computing system made up of a number of simple highly interconnected processing elements (PEs) -neurons-, which process information by its dynamic state response to external inputs.[7] Contrary to the conventional computer modeling approach, which relies on solving the equations, ANN learns by example and they provide predictions into new states. By ANN technique, instead of solving complex governing equations of the system of interest, it is possible to train the PEs using a set of input/output pairs that are representative of the physical process.

In the literature there exist several promising attempts of using ANN for chemical kinetics calculations. Choi[8] trained an ANN architecture for ignition delay time calculations where they used temperature, pressure, equivalence ratio and exhaust gas re-circulation as input for their predictions. Later, a well mixed reactor calculation was performed which was coupled with the ANN to obtain the ignition delay time rather than performing direct integration of the chemical kinetics mechanism. It was reported that a speed-up of 600 was obtained by using ANN as opposed to doing direct integration. The main problem associated with ANN computations is the generation of train/test data-set which covers the chemical state space of interest. Several different approaches are introduced in the literature, such as parametrizing the state space with respect to the mixture fraction,[9] or defining the limits of the major representative species of the mixture and assigning random values to them, which would allow to calculate the minor species as well.[10] The first approach was tested on a plug flow reactor calculation where a speed-up of 2700 was obtained against the direct integration. The predictions obtained with the latter approach was compared with a tabulated chemistry technique. It is reported that the memory requirement for such an ANN computation requires only 24 kbytes as opposed to 19934 kbytes for tabulated chemistry calculations. Finally an integration of ISAT with ANN was also studied by Chen,[11] where ANN was trained based on an already existing ISAT table. Same approach was later re-visited by Kapoor[12] and was applied to a turbulent premixed flame calculation. Although these were first succesfull attempts of integrating ANN into a turbulent flow computation, the generation of an ISAT table and training ANN based on that requires performing the simulation twice which would increase the overall effort spent on the same simulation. Current paper is seeking for a more robust way of constructing the chemical state space to train the ANN and thus using its unique capability to extract information from this data.

II. Mathematical Formulation

II.A. LES Modeling

An LES approach has been employed with a subgrid mixing and combustion model for the current calculations. For this purpose, the fully compressible, unsteady, multi-species Favre-filtered Navier Stokes equations for continuity, momentum, total energy and species conservation are used as:

$$\begin{aligned}
\frac{\partial \bar{\rho}}{\partial t} + \frac{\partial \bar{\rho}\tilde{u}_i}{\partial x_i} &= 0 \\
\frac{\partial \bar{\rho}\tilde{u}_i}{\partial t} + \frac{\partial}{\partial x_j}[\bar{\rho}\tilde{u}_i\tilde{u}_j + \bar{p}\delta_{ij} - \bar{\tau}_{ij} + \tau_{ij}^{sgs}] &= 0 \\
\frac{\partial \bar{\rho}\tilde{E}}{\partial t} + \frac{\partial}{\partial x_i}[(\bar{\rho}\tilde{E} + \bar{p})\tilde{u}_i + \bar{q}_i - \tilde{u}_j\bar{\tau}_{ji} + H_i^{sgs} + \sigma_{ij}^{sgs}] &= 0 \\
\frac{\partial \bar{\rho}\tilde{Y}_k}{\partial t} + \frac{\partial}{\partial x_i}[\bar{\rho}\tilde{Y}_k\tilde{u}_i - \bar{\rho}\bar{D}_k\frac{\partial \tilde{Y}_k}{\partial x_j} + \phi_{i,k}^{sgs} + \theta_{i,k}^{sgs}] &= \bar{\dot{\omega}}_k
\end{aligned} \tag{1}$$

Here, $\sim$ represents Favre averaging operator, and is calculated for a given quantity $\tilde{f}$ as $(\bar{\rho f}/\bar{\rho})$, where the overbar stands for spatial filtering using a top-hat filter. The subgrid shear stress (τ_{ij}^{sgs}), the subgrid viscous work (H_i^{sgs}), the subgrid diffusive flux (θ_{jm}^{sgs}) arises due to the filtering operation and they need to be modeled. Total energy is given as $\tilde{E} = \tilde{e} + \frac{1}{2}\tilde{u}_k\tilde{u}_k + k^{sgs}$, where $\tilde{e}$ is the filtered internal energy, k^{sgs} is subgrid scale kinetic energy. The filtered pressure is calculated by the filtered equation of state as $\bar{p} = \bar{\rho}R\tilde{T}$,

where R is the mixture gas constant.

For momentum and energy transport, the major effect of the small scales is to provide dissipation for the energy cascade. Therefore, an eddy viscosity type subgrid model is suitable for the calculation of subgrid stresses, τ_{ij}^{sgs} and enthalpy flux, H_i^{sgs}. The subgrid scale eddy viscosity is calculated as $\nu_t = C_\nu (k^{sgs})^{\frac{1}{2}} \bar{\Delta}$, where $\bar{\Delta}$ is the grid cut-off scale. An additional transport equation for the subgrid scale kinetic energy k^{sgs} is solved, which is in the form of:

$$\frac{\partial \bar{\rho} k^{sgs}}{\partial t} + \frac{\partial}{\partial x_i}(\bar{\rho}\tilde{u}_i k^{sgs}) = P^{sgs} - D^{sgs} + \frac{\partial}{\partial x_i}(\frac{\bar{\rho}\nu_t}{Pr_t}\frac{\partial k^{sgs}}{\partial x_i}) \tag{2}$$

where $P^{sgs} = -\tau_{ij}^{sgs}\frac{\partial \tilde{u}_i}{\partial x_j}$ represents the production term, and $D^{sgs} = C_\epsilon \bar{\rho}\frac{(\tilde{k}^{sgs})^{\frac{3}{2}}}{\Delta}$, is the dissipation term. The subgrid scale terms are closed as $\tau_{ij}^{sgs} = -2\bar{\rho}\nu_t(\tilde{S}_{ij} - \frac{1}{3}\tilde{S}_{kk}\delta_{ij}) + \frac{2}{3}\bar{\rho}k^{sgs}\delta_{ij}$, and $H_i{}^{sgs} = -\bar{\rho}\frac{\nu_t}{Pr_t}\frac{\partial \tilde{H}}{\partial x_i}$. Here, $Pr_t = 1$, and the two coefficients, $C_\nu$and C_ϵ have constant value of 0.067 and 0.916, based on an earlier calibration.[13] Also based on earlier studies, the subgrid viscous work, σ_{ij}^{sgs}, is neglected for the current LES.

II.B. Subgrid Combustion Modeling

The subgrid mass flux, ϕ_{jm}^{sgs}, the subgrid diffusive flux θ_{jm}^{sgs}, and the filtered reaction rate $\bar{\dot{\omega}_k}$ all require closure as well. However, a closure at the resolved scale (as done for momentum and energy transport) is not appropriate since combustion, heat release, volumetric expansion and small-scale turbulent stirring all occur at the small scales, which are not resolved in a conventional LES approach. To address this important physics, in our study a subgrid combustion model based on the Linear Eddy Mixing (LEM)[14] model is used to model combustion occurring within every LES cells (called LEMLES, hereafter). With this approach, there is no need to provide explicit closure for ϕ_{jm}^{sgs}, θ_{jm}^{sgs}, and $\bar{\dot{\omega}_k}$ since a more accurate and exact closure is implemented within the subgrid scales. LEMLES methodology and its ability has been reported extensively elsewhere,[15–17] however, for completeness we give a brief overview of the methodology below.

Consider the following exact transport equation for the kth scalar Y_k, where there is no LES filtering:

$$\rho\frac{\partial Y_k}{\partial t} = -\rho[\tilde{u}_i + (u'_i)^R + (u'_i)^S]\frac{\partial Y_k}{\partial x_i} - \frac{\partial}{\partial x_i}(\rho Y_k V_{i,k}) + \dot{\omega}_k \tag{3}$$

In the above equation, $V_{i,k}$ is the k-th species diffusion velocity that is obtained using Fick's law. To describe the LEMLES approach, the convective velocity is separated into three parts as: $\tilde{u}_i + (u'_i)^R + (u'_i)^S$ that represent respectively, the LES resolved velocity field, the LES resolved subgrid fluctuation (obtained from k^{sgs}), and the unresolved subgrid fluctuation. Using this definition, Eq. (3) can be recast into the following two-step numerical form:[17]

$$\frac{Y_k{}^* - Y_k{}^n}{\Delta t_{LES}} = -[(\tilde{u}_i + u'_i)^R]\frac{\partial Y_k{}^n}{\partial x_i} \tag{4}$$

$$Y_k{}^{n+1} - Y_k{}^* = \int_t^{t+\Delta t_{LES}} -\frac{1}{\rho}[\rho(u'_i)^S\frac{\partial Y_k{}^n}{\partial x_i} + \frac{\partial}{\partial x_i}(\rho Y_k V_{i,k})^n - \dot{\omega}_k^n]dt' \tag{5}$$

Here, Eqs. (4) and (5) represent large-scale and small-scale processes, respectively, and Δt_{LES} is the LES time step. The large-scale step advects the subgrid scalar gradient using a 3D Lagrangian process that ensures strict mass conservation and preserves the small-scale scalar structure. Within each LES cell the subgrid scale processes (the integrand in Eq. (5)) represent respectively, the small-scale turbulent stirring, molecular diffusion and reaction kinetics. The integrand is solved on a 1D line embedded inside each LES cells with a subgrid resolution that is fine enough to resolve the Kolmogorov scale, η. With such a resolution, both molecular diffusion and reaction rate are closed in an exact sense and this is one of the major strengths of the LEMLES strategy. The 1D line is aligned in the flame normal or the maximum scalar gradient direction and thus, does not represent any physical Cartesian direction. More specifically, the following reaction-diffusion equation (and an accompanying energy equation) is solved on the 1D LEM line for species mass fraction:

$$\rho\frac{\partial Y_k{}^m}{\partial t^s} = F_s{}^m - \frac{\partial}{\partial s}(\rho Y_k{}^m V_{s,k}{}^m) + \dot{\omega}_k^m \tag{6}$$

Here t^s indicates a local LEM timescale and the superscript m indicates that the subgrid field within each LES supergrid is resolved by N_{LEM} number of LEM cells (i.e., $m = 1, 2, ..N_{LEM}$) along the local coordinate s (which is aligned in the direction of the steepest gradient).

In the above equation, turbulent stirring is represented by ${F_s}^m$ and is implemented using a stochastic re-arrangement events that stir the subgrid scalar fields within each LES cell. The location of stirring event is chosen from a uniform distribution and the frequency of stirring is derived from 3D inertial range scaling laws derived from Kolmogorov's hypothesis as:[18]

$$\lambda = \frac{54}{5}\frac{\nu Re_{\bar{\Delta}}}{C_\lambda \bar{\Delta}^3}\frac{[(\frac{\bar{\Delta}}{\eta})^{\frac{5}{3}} - 1]}{[1 - (\frac{\eta}{\bar{\Delta}})^{\frac{4}{3}}]} \tag{7}$$

where, $C_\lambda = 0.067$.[19] The eddy size (l) is picked randomly from an eddy size distribution $f(l)$ ranging from $\bar{\Delta}$ to η: $f(l) = \frac{5}{3}\frac{l^{\frac{-8}{3}}}{\eta^{\frac{5}{3}} - \Delta^{\frac{5}{3}}}$ where $\eta = N_\eta \bar{\Delta} {Re_{\bar{\Delta}}}^{-3/4}$, and $Re_{\bar{\Delta}} = u'\Delta/\nu$ is the subgrid Reynolds number.

Volumetric expansion due to heat release is implemented locally within the subgrid by expanding the LEM domain. Although not required, re-gridding is employed to keep the total number of LEM cells constant throughout the simulation to reduce programmatic complexity. Re-gridding can introduce some numerical diffusion that is shown to be negligible in compressible flow simulations using an explicit time step Δt_{LES} (which is limited by acoustic time scale).

Once the subgrid evolution has occurred, large-scale advection (Eq. 4) is implemented by a 3D Lagrangian process that determines the amount of mass to be advected and explictly advecting this amount (and the accompanying subgrid scalar fields) across the LES cell faces. Further details of this process is given elsewhere.[17] Finally, the LES-filtered species mass fractions $\tilde{Y}_k$ (used in the LES equations) are obtained by Favre averaging the subgrid mass fractions, ${Y_k}^m$:

$$\tilde{Y}_k = (1/\sum_{m=1}^{N_{LEM}} \rho^m) \sum_{m=1}^{N_{LEM}} (\rho Y_k)^m \tag{8}$$

II.C. Chemical Kinetics and ANN

For a set of elementary reactions containing an arbitrary number of reactants N, and products M, the net rate at which species X_k is produced and/or consumed, the reaction rate, can be calculated by using the following formula:

$$\dot{\omega_k} = \sum_{i=1}^{L} \nu_{ki} q_i \tag{9}$$

where L is the number of reactions that species X_k is involved. Here, q_i is the rate-of-progress variable and calculated as:

$$q_i = k_{fi} \prod_{k=1}^{N} [X_k]^{{\nu_{ki}}'} - k_{bi} \prod_{k=1}^{M} [X_k]^{{\nu_{ki}}''} \tag{10}$$

and $\nu_{ki} = ({\nu_{ki}}'' - {\nu_{ki}}')$. The reaction rate calculation through Eq. (9) provides the link between the chemical kinetics and the subgrid scale evolution of the species that was given in Eq. (6).

The rate coefficients of the forward and backward reactions, k_f and k_b, are functions of temperature. They represent the frequency of molecular collision between molecules and probability that a collision will lead to a chemical reaction. The rate coefficients are expressed in the Arrhenius form as, $k_f(T) = B_f T^{n_f} exp[\frac{-E_{a,f}}{RT}]$, where $E_{a,f}$ is the activation energy for the forward reaction, B_f is the frequency factor, and n_f is the temperature exponential. As a result, the chemical kinetics calculations require the solution of a non-linear, coupled system of ODEs. The main problem associated with the solution procedure is the stiffness of the system of equations. Minor species have several order of magnitude different time scales than the major species which prohibits application of standard ODE solvers.[20] Thus, chemical kinetics calculations involves stiff ODE solvers, such as DVODE, that lead to a time consuming procedure.

From a chemical kinetics point of view the reaction rates are functions of the temperature, pressure and species mass fractions and the nonlinear system of equations used to determine the reaction rates can be represented as $\frac{\partial Y_i}{\partial t} = f(T, P, Y_1, Y_2, ..., Y_{NSPECI})$. From an ANN point of view, it is possible to map inputs (T, P, Y_i) to the reaction rates without requiring any knowledge for the system of equations and considering it as a ″black box″. The calculations that will be presented within the paper relies on this fact and the procedure for training the ANN and its application more specifically will be explained in the following sections.

III. Results and Discussion

III.A. ANN Code Validation

For this particular study a multilayer perceptron type of artificial neural network (MLP-ANN) is used to replace chemical kinetics calculations. A back-propagation[6] algorithm, which is essentially based on the gradient descent procedure , is used for data training. For a back-propagation type of training procedure of MLP-ANNs the algorithm basically consists of two parts: (i) forward propagating the input and (ii) backward propagating the error. Within this context, the output of a single neuron i at an arbitrary layer n can be calculated as: ${y_i}^n = g({net_i}^n)$, where ${net_i}^n = \sum_{m=0}^{M} {W_{im}}^n {y_m}^{n-1}$, M is the number of neurons connected to neuron i, g is the activation function, ${W_{im}}^n$ is the coefficient of the connection between neurons i and m at layers n and n-1, and ${y_m}^{n-1}$ is the output of the neuron m at layer n-1. Once the output of each neuron has been found, the calculation of the error associated with each neuron at the output layer is trivial and given as $E_i = \frac{1}{2}\sum_{i=1}^{I} [{d_i}^k - {y_i}^k]$, where ${d_i}^k$ is the desired output and ${y_i}^k$ is the actual output of neuron i at the output layer k. The gradient descent rule involves adjusting the connection weights according to the gradient of the local error across each connection as $\Delta w = -\eta \bigtriangledown E$, where η is the learning coefficient. Considering the fact that the error function at the output layer is differentiable, with a help of little algebra, the derivative of the local error with respect to the connection coefficient can be obtained for a connection between output and hidden layer as

$$\frac{dE}{d{w_{ij}}^k} = -[{d_i}^k - {y_i}^k] g'({net_i}^k) {y_j}^{k-1} \tag{11}$$

and for the rest of the connections as

$$\frac{dE}{d{w_{ij}}^{k-1}} = -[\sum_{l=i}^{L} \delta_l {w_{li}}^k] g'({net_i}^{k-1}) {y_j}^{k-2} \tag{12}$$

δ_l is the local error term of PE l. Its value can be calculated as: ${\delta_l}^k = [{d_l}^k - {y_l}^k] g'({net_l}^k)$ for k denoting the output layer and as: ${\delta_l}^k = g'({net_l}^k) . \sum_{z=0}^{Z} {W_{zl}}^{k+1} {\delta_z}^{k+1}$ for the hidden layer.

In this study a back-propagation type of MLP-ANN code has been written in FORTRAN, which employs the formulation described above. The ANN implementation of the gradient descent theory is slightly different than its original version and has (i) batch update and (ii) momentum term options.[21] The batch update relies on updating the coefficients based on cumulative error function, which is basically sum of the local error of a single PE obtained through certain number of iterations. This allows us to calculate new coefficients after introducing several input output pairs. Momentum term, on the other hand, is used for accelerating the convergence of the ANN by adding a portion of the previous value of the connection coefficient to its new value. The training data is introduced randomly to the net in order to avoid ANN to memorize the specific pattern, and to generalize on the nature of the process.[6] The learning coefficients associated with each hidden layer are held constant for this study. The implementation of a more generic approach, which allows calculation of the learning coefficients for each of the individual PEs dynamically by using the Delta-Bar-Delta[22] or Extended-Delta-Bar-Delta[21] did not lead into a drastic improvement in the training phase, and these options will be re-visited later.

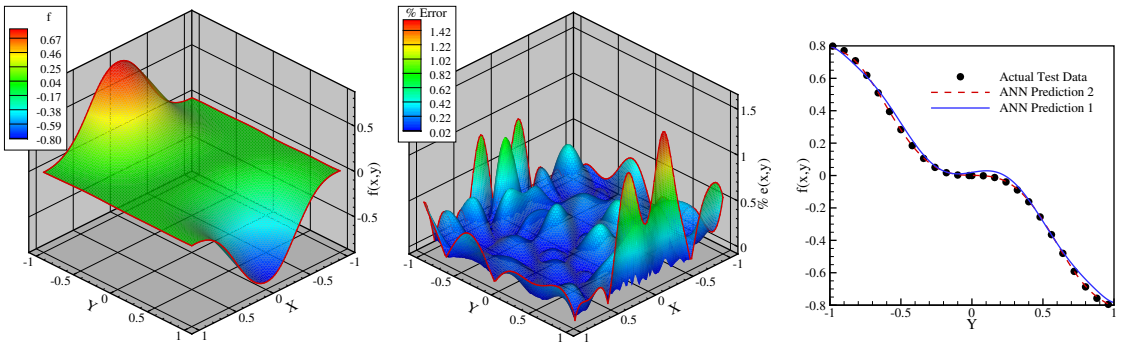

(a) Surface plot of the prediction obtained by ANN

(b) Error surface between the ANN prediction and the actual data

(c) Effect of the number of training data on predictions

Figure 1. Validation of the ANN code on a simple test function

The validity of the ANN training code is first tested on a simple function. This is an important step which proves that the ANN code is working fine and can be used as a tool for chemical kinetics calculations. The function of interest is: $f(x,y) = Sin(\pi x)^3.Cos(\pi y)^3$. The ANN training is achieved by using two different training files. First training file is constructed by 100 points, 10 in x and 10 in y, where as the second one is for 2500 points, with 50 points for each variable. The ANN architecture compromises of 3 hidden layers with 15, 10 and 4 PEs at each layer. This specific distribution is achieved by experimenting over different architectures and checking the performance with the maximum root mean square (RMS) error. The trained nets are used later to predict the function at locations for which it was not trained and the surface that is calculated with ANN is given in Fig. 1a for the net trained for 2500 points. Here, the general topology seem to be accurately captured by the ANN without any significant errors. The absolute error surface, as seen in Fig. 1b exhibits maximum values corresponding to the regions where the function reaches into its peak. For the rest of the regions, the error seem to be acceptable with a maximum value of 0.42 %. Fig. 1c shows the variation of the actual data and ANN predictions on a cross section taken in a x constant plane. As it can be clearly seen in the figure, the net trained for 100 points fails to predict the exact profile especially on the center region where it should be flat. The other net that is trained for 2500 points, on the other hand, is very accurate and follows the correct profile in a better way.

III.B. Laminar Premixed Flame Computation

Applicability of the ANN for substituting the chemical kinetics solver is first tested for a simple laminar 1-D premixed flame computation. A PSI syngas mixture[23] is used as the fuel which includes CO_2 and H_2O as diluents in a CO-H_2 fuel mixture. The main fuel components exhibit distinct reaction pathways. Hence, combustion simulations for syngas mixtures require relatively large chemical kinetics mechanisms to capture the correct physics,[24] which increases the computational cost. ANN can be used to decrease the cost for these calculations.

The initial test/train data required for ANN procedure is generated by using PREMIX module of CHEMKIN for an equivalence ratio of 0.6, and a 14 species, 10 step reduced mechanism is used for representing the chemical kinetics. The mechanism is accurate for a wide range of operating conditions of syngas flames.[25] Result obtained from the PREMIX calculation resolved the flame on 256 points. Although an exact definition for the number of train/test data is not given in the literature, it is advised that for an MLP-ANN to generalize properly, the number of independent weights need to be fewer by a factor of 10 than the number of input/output training points.[6] Considering the fact that number of PEs used for most of the previous ANN-chemical kinetics calculations is on the order of 10, 5000 points for the current computation is appropriate for the training procedure. Thus, the profiles are populated to 5000 equi-distance data points and among these points randomly 70 % is selected for training and 30 % for testing. Similar to the selection

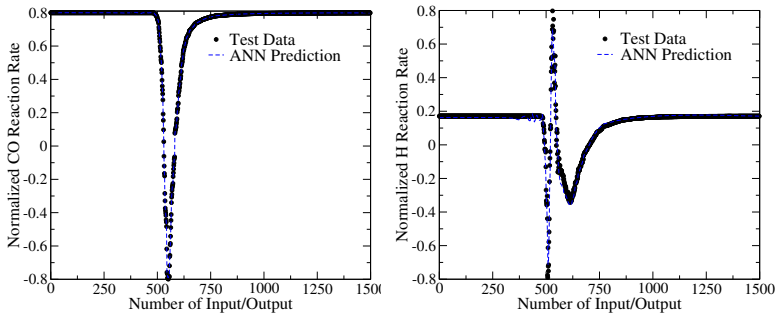

(a) CO reaction rate (b) H reaction rate

Figure 2. Actual test data and ANN predictions

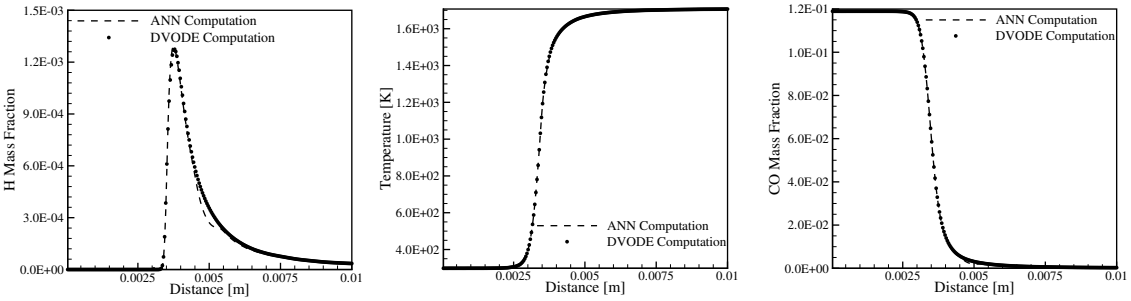

(a) H mass fraction (b) Temperature (c) CO mass fraction

Figure 3. Application of ANN to a laminar, time dependent syngas-air flame

of exact number of training points, the relative percantage of train and test data is also case dependent, and the range varies between 60-80 % in the literature.[8,9] The ANN architecture for this particular case consists of 15 inputs and 3 hidden layers with each having 20, 10 and 8 PEs, respectively. The optimum value for the architecture is defined by experimenting with different values of PEs at the hidden layers and checking the performance of the ANN for predicting the test data. The architecture used for this study corresponds to an RMS error at the outpur layer of 0.56 % at maximum for the OH radical. The errors associated with other species are less than this value, e.g., the maximum RMS error for H_2 is 0.073 %. 14 independent nets are generated for the reaction rates of each species. Following the information given in the literature,[21] in order to avoid saturation at the output layer, the normalized reaction rate is scaled to vary between $\pm$ 0.8 as opposed to the normalized input, which is between $\pm$ 1. The comparison of the ANN predictions and the actual test data is shown in Fig. 2a and b. In general, reaction rates exhibit two distinct profiles depending on the species. Major species, such as CO, H_2, CO_2, H_2O for this particular case, are either consumed or produced at all in the flame region corresponding to a profile as given in Fig. 2a. The minor species, on the other hand, are consumed and produced in the flame region. A typical example for this kind of behavior is given in Fig. 2b. It is crucial and must be proved that ANN is able to predict both profiles correctly, which is the case for this calculation. For this purpose, the performance of the net has been tested on the data that it was not trained for as shown in Fig. 2a, b with the dashed lines. For both of these species ANN succesfully captures the correct profile, except for small oscillations in H reaction rate right before it starts to decrease. This defect is very small and the RMS value averaged for all the input/output pairs at the at

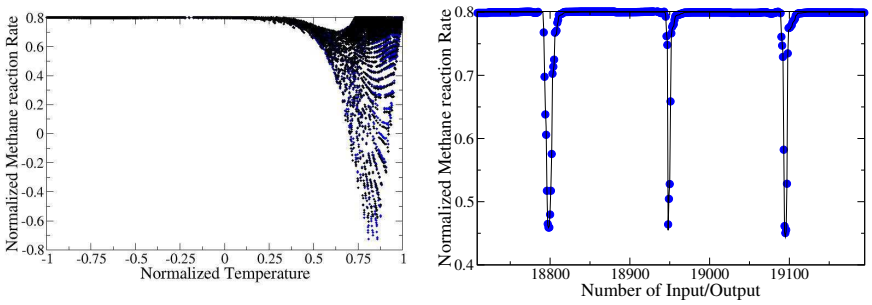

(a) Test data and ANN prediction-for all equivalence ratios

(b) Test data and ANN prediction-close-up view of 3 equivalence ratios

Figure 4. Actual test data and ANN predictions for ANN-MER approach applied to a methane-air flame

the output layer is less that 1 %, which is a good indicator of the accuracy of the ANN.

In order to further test the performance of the ANN, a time dependent computation is performed by creating an ANN module for chemical kinetics calculations in an existing flow solver. For this purpose, the profiles obtained by PREMIX calculation is used to initialize a 3-D computation. The initial PREMIX profile is linearly interpolated onto a uniform grid of 256 points in the x direction. The same profile is later replicated to all y locations, and the $x-y$ plane is copied to all z locations, resulting a grid of 256x12x2 points in x, y and z directions, respectively. The profiles obtained by such a calculation is given in Fig. 3a-c for H, CO mass fraction and temperature. As to yield a better comparison the DVODE calculations are also presented in the figures. The H mass fraction exhibits small discrepancey approximately at 0.005 m. Although not shown here, this defect shows itself for some other minor species too, but major species in general are free from this problem. The error does not impact the resolved flame, as shown in the temperature plot.

III.C. Flame Turbulence Interaction

III.C.1. Methane-Air Flames

Computation for a simple steady-state, laminar case is carried out to demonstrate that the developed ANN model for chemical kinetics predictions is working. However, the realistic combustor applications are generally highly turbulent and unsteady problems. LES computations are widely used for the reactive flow analysis and the goal of the current section is to check the applicability of ANN to be used as a chemistry integrator for LES computations. For this purpose, following an earlier LES[26] and DNS[27] study that exist in the literature we consider a premixed methane-air flame front interacting with an initially generated isotropic turbulent flow field. Similar to the previous section, the LES is initialized by using the solution of PREMIX-CHEMKIN and the flame is at a lean condition (ϕ=0.8) with the reactants initially preheated up to 570 K. Based on the initial turbulence level and the flame properties, the premixed flame is in the thin reaction zone (TRZ) regime. A 5 species ($CH_4, O_2, CO_2, H_2O, N_2$), 1 step reduced methane-air chemical kinetics mechanism is used for ANN training and LES computations. Following the earlier LES,[26] the subgrid scale combustion processes are simulated with LEM by using 12 grid points inside each LES cell.

Two different ANN training procedure has been used for this section of the study. First one is based on generation of train/test data-set for a single equivalence ratio (SER), similar to what was done for the laminar computations. The second method, on the other hand, relies on training ANN for multiple equivalence ratios (MER), so as to cover a larger portion of the chemical state space. This is particularly important for turbulence computations with thermally perfect and mixture transport properties, since small perturbations can change the composition space locally. The procedure of ANN training based on a SER is exactly similar to the procedure outlined in the previous section. The solution of PREMIX is populated to

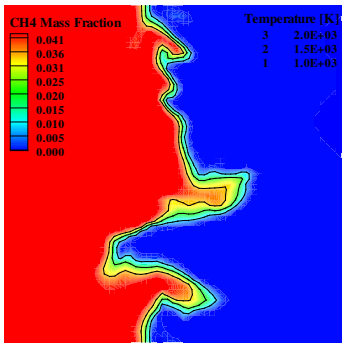

(a) CH_4 mass fraction surface plot and temperature contours for DVODE computation

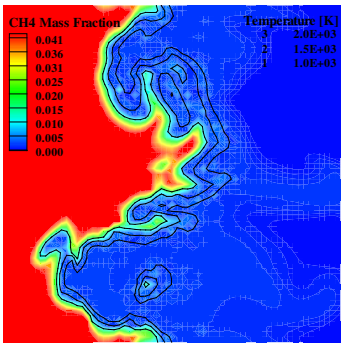

(b) CH_4 mass fraction surface plot and temperature contours for ANN-SER computation

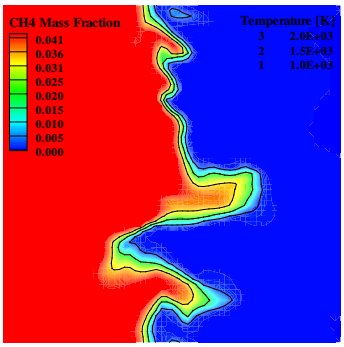

(c) CH_4 mass fraction surface plot and temperature contours for ANN-MER computation

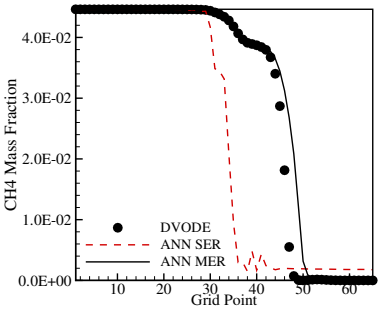

(d) CH_4 mass fraction profile comparison at cross-section A-A

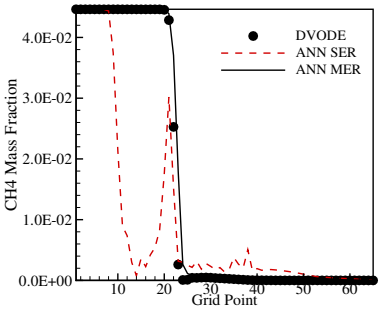

(e) CH_4 mass fraction profile comparison at cross-section B-B

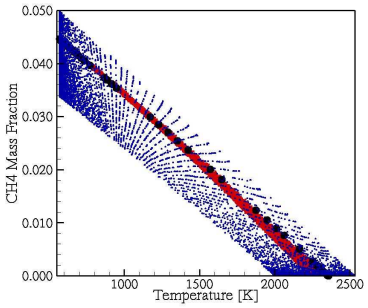

(f) Composition state-space accessed by SER, MER training approaches and DVODE computations

Figure 5. Application of ANN to a turbulent premixed methane-air flame

1000 points and several ANN architectures are used to determine which one is better on predicting the test data. Although it is generally advised to employ 1 or 2 hidden layers at most,[21] for this particular study 2 hidden layer configuration was the worst case and an ANN architecture with 1 input, 1 output and 3 hidden layers each having 8, 4 and 2 PEs, respectively, is constructed. Based on the second training approach, a database of 1-D laminar premixed flame solutions for equivalence ratios ranging from 0.60 to 0.9 with increments of 0.001 is generated. The PREMIX solution for each equivalence ratio compromises 50 points which is interpolated to 500. ANN results based on the test data which is a part of the training procedure is given in Fig. 4a-b. Fig. 4a, shows the ANN predictions and actual test data on the CH_4 reaction rate - Temperature hyperplane of the chemical state space. Here, the ANN predictions are comparable with the actual test data and it is not possible to distinguish between both of them for most of the region. The only considerable amount of disrcepancy occurs at the region where reaction rate is at maximum. The reason for this is, this region is accessed only by couple of equivalence ratios, thus, is not well populated. A comparison of the profiles with respect to the equivalence ratios is presented in Fig. 4b, where the agreement is quite accurate.

Results obtained by using DVODE, ANN-SER and ANN-MER computations after 4 flow through time is introduced in Fig. 5. Here, 1 flow through time is defined as l/u', where l is the largest eddy size and u' is the turbulent fluctuation. The effect of different turbulent scales on the scalar field evolution is evident in the

Table 1. Simulation parameters for flame turbulence interaction problem

	u'/S_L	l/l_f	Regime [m]	Box Size [cm]
FTI-Case 1	10	5	TRZ	3.0
FTI-Case 2	5	5	TRZ	5.0

Table 2. Flame Parameters used for flame turbulence interaction

	Fuel Composition	Equivalance Ratio	S_L [m/s]	l_f [m]
H_2:CO:CO_2:H_2O	0.0678:0.113:0.0254:0.0650	0.6	0.2105	8.755×10^{-4}
O_2:N_2	0.1507:0.5781			

CH_4 mass fraction surface plot obtained by DVODE computations as shown in Fig. 5a. The temperature contours covers the maximum value of the CH_4 on a thin region indicating the flame zone. This feature is absent in the ANN-SER computations as given in Fig. 5b. The temperature contours seem to be spread out, covering a larger area across the flame front. Also, the flame topology seems to be very different than the DVODE calculations and do not exhibit any similar structure. On the other hand, ANN-MER computations predict a very similar flame topology with DVODE calculations as shown in Fig. 5c.

A better understanding of the effect of different ANN training approaches can be achieved by investigating the actual profiles along a cross section of the flame and is introduced in Fig. 5d-e. The profiles are obtained across the flame front at y= 0.0125 m and 0.0101 for Fig. 5d and e, respectively. These locations correspond to a convex and a concave region of the flame. The ANN-MER computation as seen in Fig. 5d, predicts a slightly larger flame region as opposed to DVODE. In Fig. 5e, on the other hand, the agreement is better. As it was observed in the surface plot, the predictions obtained by ANN-SER, is very different than the DVODE results and look unphyisical. The region on the CH_4 mass fraction and temperature hyperplane of the chemical state-space that is accessed by DVODE computations and covered by the ANN MER-SER training procedures is shown in Fig. 5f. Here, the ANN-SER results are shown with black circles and it corresponds to a line on the state-space. The actual data obtained by DVODE computations is not a single line, but it covers a region within the state-space. The ANN-SER approach, therefore, can not provide predictions, since the region of interest is outside of its training region. The ANN-MER approach covers a larger space on the state-space which is more general and adapts itself to local perturbations in the composition state space in a better way.

III.C.2. Syngas-Air Flames

The applicability of ANN into flame-turbulence interaction computations by using LEMLES is studied further in a configuration with an embedded pair of coherent vorticies in an isotropic background turbulence, where there is wrinkling of the flame surface both by large and small scales. More specifically a flame front interacting with a pair of spanwise vorticies superimposed on an isotropic turbulent premixed mixture is of interest. This is more difficult test case as large scale wrinkling alters significantly the diffusion of the species across the flame front. $uc, max/S_L$ and D_c/l_f for this vortex pair is 50 and 5, respectively. The fuel composition and the size of the coherent structure are held constant, and in connection with an earlier study.[28] Two different background turbulence levels are simulated, where the flames are in the thin-reaction-zone (TRZ) regime. A 64^3 grid is used for all cases, and the size of the computational domain is selected as to yield a minimum spacing of 3.3 times the Kolmogorov length scale. In the subgrid level within each LES cell, 12 LEM cells ($N_{LEM} = 12$) are used, which allows a resolution of 4 times smaller than η. The fuel composition is PSI as defined by General Electric.[23] Simulation parameters and flame properties for FTI computations are summarized in Tables 1 and 2, respectively.

As it was shown in the previous section, since an ANN-MER approach is superior to ANN-SER, the ANN training approach here uses only the MER technique. The training data is constructed for equivalence ratios ranging from 0.45 to 1.10 with jumps of 0.005. Also, to avoid poor training due to the few number

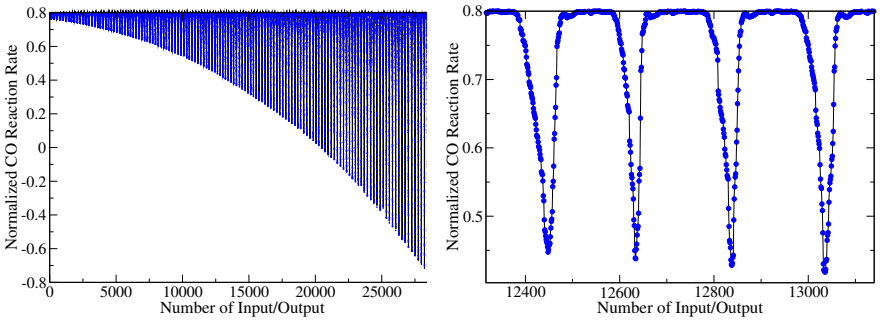

(a) Test data and ANN prediction-for all equivalence ratios

(b) Test data and ANN prediction-close-up view

Figure 6. Actual test data and ANN predictions for an ANN-MER approach applied to a syngas-air flame

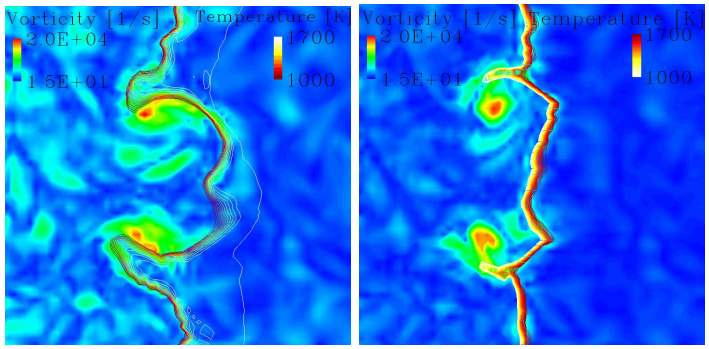

(a) Vorticity surface plot and temperature contours for Case 1

(b) Vorticity surface plot and temperature contours for Case 2

Figure 7. Application of ANN to a turbulent premixed syngas-air flame

of data points associated with each single equivalence ratio, the gridding sensivity of PREMIX is increased by adding more grid points to sections where there are large gradients, which yielded approximately 700 points. In total, there is 67128 train and 28768 test data. The ANN architecture consists of 5 layers, having 3 hidden layers with 20, 10 and 8 PEs, respectively. The exact ANN architecture is constructed following the same logic that was outlined in the previous sections. The test data and the ANN predictions for the normalized CO reaction rate is given in Fig. 6a. The data corresponds to an almost non-smooth function of the reaction rate with respect to the equivalence ratio. The ANN can, however, predict the profile fairly well. A close-up look of the profiles reveal that as there are more train/test points for each equivalence ratio, the ANN predictions match with the actual data better than the earlier case. Although it can not be detected well in these figures, the only considerable amount of difference between ANN predictions and the test data is at the regions where there is not any reaction rate which corresponds to a value of 0.8 on the normalized data. ANN fails to predict an absolute zero value of reaction rate in the post and pre flame regions. This problem is overcome by adding a threshold to the ANN value, beyond which the reaction rates are considered to be zero.

The LESLEM results obtained for both cases by employing ANN approach are given in Fig. 7a-b at a non-dimensional time of 0.3. The time is non-dimensionalized with the characteristic time, which is calculated based on the backgorund turbulence level as D_c/u'. Here, Figs. 7a and b shows the contour plot

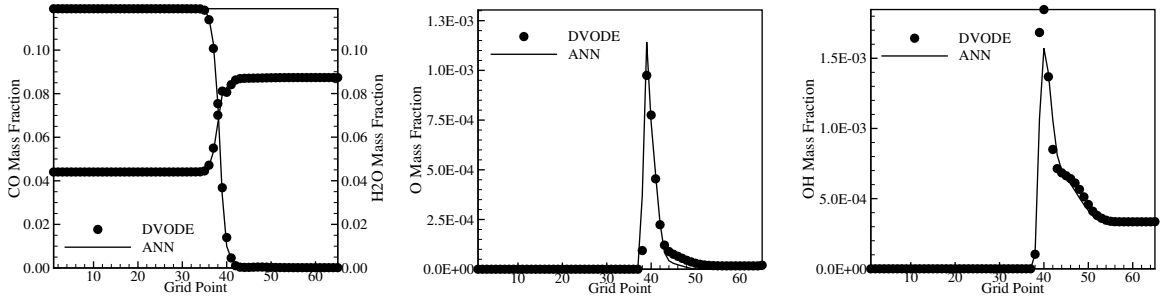

(a) CO and H_2O mass fraction for Case 1

(b) O mass fraction for Case 1

(c) OH mass fraction for Case 1

Figure 8. Comparison of species profiles obtained by DVODE and ANN approaches for turbulent, premixed syngas-air flame, Case 1

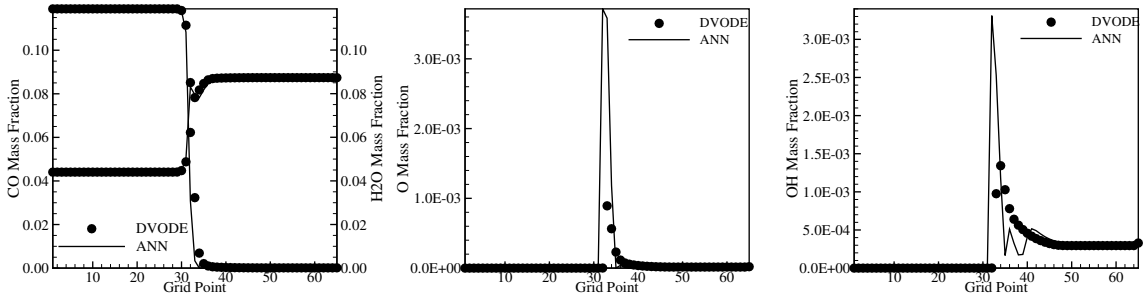

(a) CO and H_2O mass fraction for Case 2

(b) O mass fraction for Case 2

(c) OH mass fraction for Case 2

Figure 9. Comparison of species profiles obtained by DVODE and ANN approaches for turbulent, premixed syngas-air flame, Case 2

of temperature superimposed on the vorticity surface plot. The flame front is wrinkled both by the large scale-coherent vortex pair and the small scale background isotropic turbulence. The small-scale vorticity in the incoming turbulent field dissipates across the flame and only the large structures exist in the burned side due to the high temperature values in this region. A detailed description of the interaction between the flame and the vortical structures is given elsewhere.[28] The comparison of the computed profiles across the flame is given in Fig. 8a-c for Case 1. The profiles obtained for major species CO and H_2O match well with the DVODE computations. The minor species, O and OH, show discrepancy near the peak region. The maximum error for both of the species is less than 18 %. However, both species mass fraction is on the order of 10^{-3} and the impact of their error is not very severe on the major features of the flame.

The agreement between the profiles obtained for flame Case 2, as shown in Fig. 9a-c, however, is not as good as it is obtained for Case 1. CO starts to be consumed earlier than that is calculated with DVODE and the H_2O mass fraction exhibits a peak value within the flame zone. The maximum value of the minor species is overpredicted, almost 4 times for O and 2 times for OH. The profile for OH also corresponds to an oscillation which is not physical. In order to gain further insight into the effect of ANN on the LEMLES computations, the $CO_2 - OH$ hyperplane of the chemical state-space is presented in Fig. 10. Here, Fig. 10a corresponds to the region that was accessed by DVODE, whereas Fig. 10b is by the ANN calculations. In

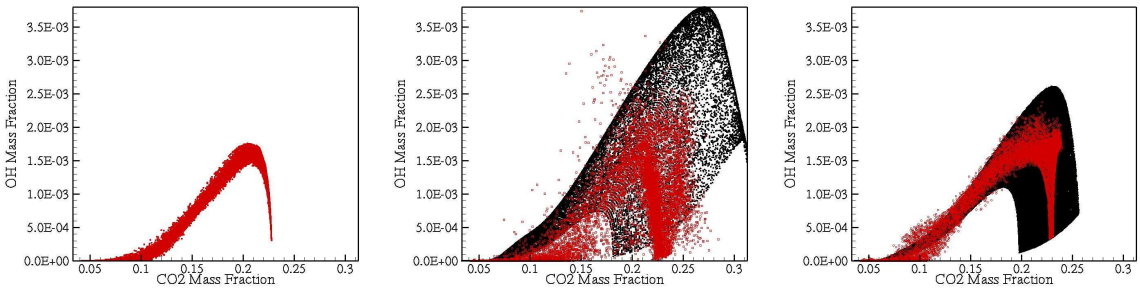

(a) Actual sample space accessed by DVODE computation

(b) Training data for ANN and the actual sample space accessed by ANN computations

(c) Refined training data for ANN and the actual sample space accessed by ANN computations

Figure 10. $CO_2 - OH$ **Hyperplane Accessed during computations and training Phase**

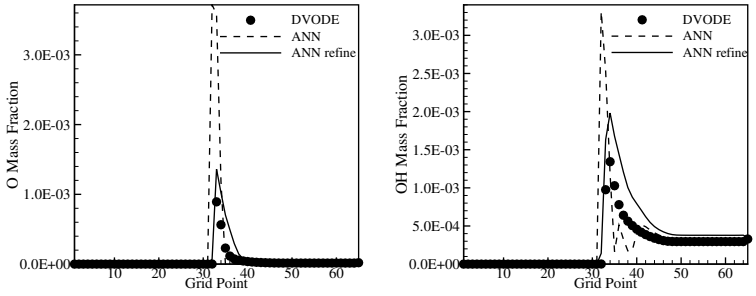

(a) O mass fraction profiles by DVODE and ANN computations for Case 2

(b) OH mass fraction profiles by DVODE and ANN computations for Case 2

Figure 11. Comparison of species profiles obtained by DVODE and ANN approaches for turbulent, premixed syngas-air flame, Case 2 with refined table

Fig. 10b, the region that was covered within the initial ANN training phase is also given, and denoted with black dots. The DVODE computations, similar to that was obtained for earlier methane-air case, supports the idea why it is not possible to achieve training and expect accurate results for a SER computation. This time, rhe region is more complex and can not be represented by a SER, which would actually correspond to a single line on the hyper-plane. A direct comparison of the region covered by the ANN training phase and the actual region constructed by DVODE computations reveal that only a single portion of the state-space is actually accessed. Since the ANN is trained for a wide range, the accessed points with the ANN computation is spread over the entire region. Moreover, the ANN training table is sparse in most of the region, which would avoid ANN to fully generalize on the training data.

In order to get better solution, a new ANN training table is produced for a smaller portion of the chemical state-space but with a finer resolution. The ANN is trained for a range of equivalence ratios from 0.5 to 0.7 with 0.001 increments. The $CO_2 - OH$ hyperplane representative of the region accessed through ANN training and LEMLES computations is given in Fig. 10c. The accessed region by LEMLES for this training file is very similar to the region covered by DVODE, as shown in Fig. 10a. For low values of the CO_2, the region used for training becomes very thin and cannot cover the accessible region as predicted by DVODE

calculations. Hence, the ANN prediction spreads over a relatively larger area compared to DVODE. The species profile as seen in Fig. 9. is much better than the results in Fig. 11. There is still an overestimation of the minor species maximum value, but the error is smaller than the previous case and most importantly the profiles do not exhibit any non-physical structure. Nevertheless this is going to be studied further for future study.

As it was outlined in the previous sections, most important merit of using ANN against stiff ODE solvers is its speed, and against ISAT and ILDM based look-up table approaches is its efficiency in terms of memory. The time required for one time step iteration for the laminar, premixed syngas-air flame simulation with DVODE is 0.21547 sec and for ANN is 0.06217, which corresponds to a speed up of 3.47. The size of the table that is used for the training procedure is 23.8 MB. For the turbulent syngas-air flame simulation, the time required for one iteration is 42.7969 sec for DVODE and 11.62101 sec for ANN, which approximately corresponds to the same amount of speed up, 3.68. For the turbulent flame simulation, compared to the laminar flame, the memory required for the ANN training is larger since a MER approach is employed. The table that is used for training is 522.6 MB and hence, using ANN saved a considerable amount of memory. Finally, for the turbulent methane-air flame a speed up of 1.98 is achieved. The reason why the amount of speed up decreased compared to the syngas-air flames is related with the reduced mechanism that is used. The chemical kinetics calculations for the methane-air calculations are made by using a small, 1 step 5 species reduced mechanism. Thus, the time required for the solution of the stiff ODE is not as huge as it is for the syngas flame. Still, ANN saves a 93.4 MB of memory.

IV. Conclusion

Calculation of the changes in the chemical state-space due to the reactions, relies on employing stiff ODE solvers. This approach may be very time consuming if the chemical kinetics mechanism used for the simulations involves many species and steps. Look-up table approach, on the other hand, can be used for decreasing the cost, but the memory requirement for this approach is usually huge. The current paper seek for an optimal solution into this problem by using ANN approach. It has been showed that, in contrast to employing stiff ODE solvers, ANN is very time effective, and the memory requirement is not as large as it is for look-up table approach. The focus of the paper has been spent for the determinig the reliability of the ANN predictions, which is highly dependent on the training procedure. For premixed flames it has been showed that the ANN can be trained based on the solution of a 1D laminar premixed flame. This approach, however, is not very effective for turbulent computations, since turbulence may perturb the composition state-space locally which would not let it to be represented simply by one equivalence ratio. Training based on multiple equivalence approach yielded better results as it has been shown for turbulent, premixed methane-air and syngas-air flames. As long as the composition state-space is covered with sufficient number of chemical states, ANN can be used succesfully for replacing stiff ODE solvers.

As for the next step of incorporating ANN into LES computations for decreasing the computational time without sacrificing the accuracy is to use it as a subgrid scale combustion model. This would involve more complicated ANN architecture but would drastically decrease the computational cost. The study is still underway.

Acknowledgements

The authors would like to acknowledge Prof. J.-Y. Chen for providing the reduced chemical kinetics reaction mechanism for syngas that was used in this study.

Appendix

IV.A. 10 Step reduced Chemical Kinetics Model

Species:H_2, H, O, OH, HO_2, H_2O, CO, O_2, H_2O_2, CO_2, CH_4, CH_2O, NO, N_2

$H + O_2 = O + OH$

$H_2 + O = H + OH$

$H_2 + OH = H + H_2O$

$2H = H_2$
$H + O_2 = HO_2$
$2OH = H_2O_2$
$O + CO = CO_2$
$O + CH_4 = 2H + CH_2O$
$O + O_2 + CH_2O = OH + HO_2 + CO$

References

[1]Goldin, G. and Menon, S., "Scalar PDF Construction Model for Turbulent Non-Premixed Combustion," *Combust. Sci. Tech.*, Vol. 125, 1997, pp. 47 – 72.

[2]Maas, U. and Pope, S. B., "Simplifying Chemical Kinetics: Intrinsic Low-Dimensional Manifolds in the Composition Space," *Combust. Flame*, Vol. 88, 1992, pp. 239–264.

[3]Pope, S. B., "Computationally Efficient Implementation of Combustion Chemistry Using In Situ Adaptive Tabulation," *Combust. Theory Modelling*, Vol. 1, 1997, pp. 41–63.

[4]Sen, B. A., Ozdemir, I. B., and Warnatz, J., "Implementation of the Hierarchical Structures of the Combustion Processes into Intrinsic Low-Dimensional Manifolds Technique," *4th International Symposium on Turbulence, Heat and Mass Transfer*, 2003.

[5]Mehrotra, K., Mohan, C. K., and Ranka, S., *Elements of Artificial Neural Networks*, MIT Press, 1997.

[6]Christodoulou, C. and Georgiopoulos, M., *Applications of Neural Networks in Electromagnetics*, Artech House, 2000.

[7]Hecht-Nielsen, R., *Neurocomputing*, Addison-Wesley, 1990.

[8]Choi, Y. and Chen, J.-Y., "Fast Prediction of Start-of-Combustion in HCCI with Combined Artificial Neural Networks and Ignition Delay Model," *Proc. Combust. Inst.*, Vol. 30, 2005, pp. 2711–2718.

[9]Blasco, J. A., Fueyo, N., C., L. J., Dopazo, C., and Chen, J.-Y., "A Single-Step Time-Integrator of a Methane-Air Chemical System Using Artificial Neural Networks," *Computers and Chemical Engineering*, Vol. 23, 1999, pp. 1127–1133.

[10]Blasco, J. A., Fueyo, N., Dopazo, C., and Ballester, J., "Modelling the Temporal Evolution of a reduced Combustion Chemical System With an Artificial Neural Networks," *Combust. Flame*, Vol. 123, 1998, pp. 38 – 52.

[11]Chen, J. Y., Blasco, J. A., Fueyo, N., and Dopazo, C., "An Economical Strategy for Storage of Chemical Kinetics:Fitting *InSitu* Adaptive Tabulation With Artificial Neural Networks," *Proc. Combust. Inst.*, Vol. 28, 2000, pp. 115–121.

[12]Kapoor, R., Lentati, A., and Menon, S., "Simulations of Methane-Air Flames Using ISAT and ANN," *AIAA-01-3847*, 2001.

[13]Chakravarthy, V. and Menon, S., "Large-Eddy Simulations of Turbulent Premixed Flames in the Flamelet Regime," *Combust. Sci and Tech*, Vol. 162, 2000, pp. 1–48.

[14]Kerstein, A. R., "Linear-Eddy Model of turbulent Scalar Transport and Mixing," *Combust. Sci. Tech.*, Vol. 60, 1988, pp. 391–421.

[15]Menon, S., Yeung, P.-K., and Kim, W.-W., "Effect of Subgrid Models on the Computed Interscale Energy Transfer in Isotropic Turbulence," *Computers and Fluids*, Vol. 25, No. 2, 1996, pp. 165–180.

[16]Eggenspieler, G. and Menon, S., "LES of Premixed Combustion and Pollutant Emission in a DOE-HAT Combustor," *AIAA-2003-0309*, 2003.

[17]Menon, S. and Patel, N., "Subgrid Modeling for LES of Spray Combustion in Large-Scale Combustors," *AIAA Journal*, Vol. 44, No. 4, 2006, pp. 709–723.

[18]Kerstein, A. R., "Linear-Eddy Model of Turbulent Transport II," *Combust. Flame*, Vol. 75, 1989, pp. 397–413.

[19]Chakravarthy, V. and Menon, S., "Linear-Eddy Simulations of Reynolds and Schmidt Number Dependencies in Turbulent Scalar Mixing," *Physics of Fluids*, Vol. 13, 2001, pp. 488–499.

[20]Warnatz, J., Maas, U., and Dibble, R. W., *Combustion:Physical and Chemical Fundamentals, Modeling and Simulation, Experiments, Pollutant Formation*, Springer, 2006.

[21]NeuralWare, *Neural Computing. A Technology Handbook for NeuralWorks Pro fessional II / PLUS*, NeuralWare, 2001.

[22]Jacobs, R. A., "Increased Rates of Convergence Through Learning Rate Adaptation," *Neural Networks*, Vol. 1, 1988, pp. 295–307.

[23]Bradar, R. D. and Jones, R. M., "GE IGCC Technology and Experience with Advanced Gas Turbines," Ger-4207, GE Power Systems, Schenectady, NY, October 2000.

[24]Natarajan, J., Nandula, S., Lieuwen, T., and Seitzman, J., "Laminar Flame Speeds of Synthetic Gas Fuel Mixtures," *ASME Paper*, 2005.

[25]Mosbacher, M., Haynes, J., Janssen, J., Brumberg, J., Lieuwen, T., Menon, S., Seitzman, S., and Anand, A., "Fuel-Flexible Combustion System for Co-Production Plant Applications," De-fc26-03nt41776, GE Global Research, Schenectady, NY, October 2006.

[26]Sankaran, V. and Menon, S., "Subgrid Combustion Modeling of 3-D Premixed Flames in the Thin-Reaction-Zone Regime," *Proc. Combust. Inst.*, Vol. 30, No. 1, 2005, pp. 575–582.

[27]Trouvé, A. and Poinsot, T., "The Evolution Equation for the Flame Surface Density in Turbulent Premixed Combustion," *Journal of Fluid Mech.*, Vol. 278, 1994, pp. 1–31.

[28]Sen, B. A. and Menon, S., "Large-Eddy Simulations of Turbulent Flames in Syn-Gas Fuel-Air Mixtures," *AIAA-2007-1435*, 2007.